AIChE

Simultaneous Quantitative Measurement of Gaseous Species Composition and Solids Volume Fraction in a Gas/Solid Flow

Jean-Philippe Laviolette, Gregory S. Patience, and Jamal Chaouki
Dept. of Chemical Engineering, Ecole Polytechnique, C.P. 6079, succ. Centre-Ville, Montréal, H3C 3A7, Canada

DOI 10.1002/aic.12210
Published online March 22, 2010 in Wiley Online Library (wileyonlinelibrary.com).

A novel spectroscopic method was developed to measure quantitatively and simultaneously solids volume fraction ($1-\varepsilon$) and gaseous species composition (Y_i) in a gas/solid system. The method was comprised of an FT-IR coupled to a fiber-optic probe that could perform real-time and in situ measurements of absorbance. The effect of ($1-\varepsilon$) and Y_i on the absorbance spectra were additive and could be independently calibrated. Experiments were conducted with alkane/nitrogen mixtures and two types of particles: sand and FCC. Fuel mole fractions and ($1-\varepsilon$) were varied between 1.8–10.1 mol % and 0–0.45, respectively. The relative errors for Y_i time-averaged measurements were below 6% and the error increased significantly with decreasing beam intensity. A proof of concept for a novel application in fluidized beds was also completed: the fiber-optic probe was used to measure the molar fraction of a tracer gas inside the emulsion and bubble phases during gas tracer experiments. © 2010 American Institute of Chemical Engineers *AIChE J,* 56: 2850–2859, 2010

Keywords: solids volume fraction, infrared spectroscopy, gaseous species composition, FT-IR, bubble, emulsion, fiber-optics, fluidization

Introduction

Multiphase processes are common to many industries: petrochemical, chemical, pharmaceutical, energy, food, pulp, and paper. They are also present throughout the process chain: energy generation (combustors), transformation (gasifiers, chemical reactors, mixers, and dryers), purification/separation (cyclones and precipitators), and waste disposal (chimneys). System characterization through the measurement of species composition and solids volume fraction is critical for process control, optimization, and trouble-shooting in the industries and laboratories. It is also essential for the development of hydrodynamic (gas/liquid/solid) and kinetic models. Chemical species composition and solid volume fraction are currently measured independently with two different techniques.

Several noninvasive and invasive techniques have been developed to measure solids volume fraction in two- and three-phase systems. Invasive techniques involve the insertion of probes to measure the local capacitance,[1–3] conductivity,[4–6] fluorescence,[7] forward-scattering,[8] or back-scattering of light in the medium.[2,9–11] The solids volume fraction is derived from the measurement, which can be made in situ and in real-time. In liquid/solid or gas/liquid/solid systems, the slurry phase can also be sampled with special probes to measure the liquid and solids volume fraction.[7,12] Noninvasive techniques include tomography,[13–16] densitometry,[11] and the analysis of ultrasonic wave distortions.[17] These techniques produce time- or space-averaged maps of solids volume fraction in multiphase systems with varying resolution.

Species concentrations in the gas or liquid phases can be analyzed continuously or intermittently[12] with analytical instruments (chromatograph, spectrometer, etc.) via sampling. Furthermore, in the context of the US Food and Drug Administration process analytical technology initiative, several publications have reported the development of infrared (IR) applications for the measurement of chemical species composition in multiphase samples.[18,19] Similar applications have also been developed for the in situ monitoring of

Correspondence concerning this article should be addressed to J. Chaouki at jamal.chaouki@polymtl.ca.

reactions at the surface of catalysts.[20,21] These systems function in transmission and diffuse reflectance modes (on the solid surface) and can measure species composition the continuous phases (liquid and gas) as well as characterizing qualitatively the chemical composition of the discrete phase (solid particles and liquid droplets).[22–26] All these techniques measure species concentrations in the continuous phase as a spatial average between the different regions of varying solids volume fractions (e.g., bubble and emulsion phases in fluidized bed).

A technique that measures species composition and solids volume fraction simultaneously yields much more information into multiphase processes as solids volume fraction and species concentrations are dependent parameters. These two parameters are coupled through the reaction kinetics and the hydrodynamics. During the reaction, solids volume fraction influences chemical reactions through heterogeneous catalytic and/or inhibitive effects as well as through the thermal balance. Furthermore, at the hydrodynamic level, multiphase systems are often characterized by different regions of varying void fraction and the species composition in these regions are fundamental to the process characterization. For example, bubbling and turbulent gas/solid fluidized beds are characterized by a dense phase (emulsion) and a dilute phase (bubbles). Bubbles cause gas by-passing that lowers the process yield. The simultaneous measurement of solids volume fraction and gaseous species composition discriminates between the reactants in the dilute and dense phases and this measurement can hardly be made with existing methods.

IR spectroscopy offers a great potential for the simultaneous measurement of solids volume fraction and gaseous species composition. IR spectroscopic applications in multiphase systems are affected by the solid phase characteristics. The solids volume fraction and particle size have been shown to influence the interaction between the light and the solids, which affect the path length of the IR beam and the effective sample size.[20,23] An increase in particle size has been reported to decrease the fraction of scattered light and to increase penetration depth of light into the solid particles, resulting in increased absorbance and an upward shift of the absorbance baseline in diffuse reflectance spectroscopy.[23] Therefore, current IR spectroscopic applications in multiphase system rely on the uniformity of the solid samples with time (between measurements). This is achieved by performing the spectral acquisition in immobile samples, such as solid tablets.[25,27–30] On the other hand, measurements in dynamic systems (fluidized beds or mixers, for example) require shutdown before the spectral acquisition,[31,32] the synchronization of the spectral acquisition to a specific vessel position[33] or measurement in regions of high solids density.[34] Nonintrusive NIR monitoring of powder blend homogeneity has also been conducted in symmetrical mixers to ensure the temporal uniformity of the solids volume fraction when complete mixing is reached.[35] Finally, mathematical treatments of the spectra, such as the derivative treatment, are often used to minimize the effects of baseline shifts because of the changes in the solid phase properties.[23] However, multiphase systems are generally characterized by solids volume fractions that are heterogeneous in space and time. Therefore, the in situ and real-time measurement of species concentrations in the different regions of a multiphase system requires the simultaneous determination of solids volume fraction. The measurement volume can be made independent of the solid properties by inclining the emitting and receiving fibers to form a convergent scheme.[36] This principle can be applied to an IR fiber-optic probe to measure species concentrations.

In multiphase systems, the movement of powders makes spectroscopy measurements and interpretation more complex. The measured absorbance spectra are influenced by variations in the solids volume fraction and the average distance from the sample to the probe. When samples are moving, different parts of the spectrum may also be influenced to a varying degree by local heterogeneities (different material components). The effects of moving particles on Fourier-Transform spectroscopy have been investigated by De Paepe et al.,[37] Berntsson et al.,[38] and Andersson et al.[39] It was shown that the movement of the particles produced artifacts on the measured spectrum at certain wavenumbers that depended on the timescale of the spectral scan compared with the rate of movement of the particles. The wavenumber at which the artifact appeared increased with increasing modulation frequencies such that the effects of moving particles could be completely eliminated at the wavenumbers of interest with a sufficiently high modulation frequency.

In the present study, a novel spectroscopic method was developed for the simultaneous and quantitative measurement of gaseous species composition (Y_i) and solids volume fraction ($1-\varepsilon$). Experiments were conducted using near- and mid-IR Fourier transform transmission spectroscopy (6000–1000 cm^{-1}). A fiber-optic probe was constructed to perform in situ and real-time measurements in a gas/solid flow of methane/nitrogen and silica sand particles ($d_p = 290\ \mu m$). Absorbance spectra were recorded at a frequency of 4.5 Hz for a period of 75 s and both Y_i and $(1-\varepsilon)$ were evaluated from each spectrum. Methane molar fractions in nitrogen were measured over a range of 0–10.1 vol %. Furthermore, the solids volume fraction was varied between 0 and 0.1. The fiber-optic probe was also used inside a fluidized bed of FCC catalyst during gas tracer experiments to measure the tracer (CH_4) molar fraction inside the bubble and emulsion phases ($(1-\varepsilon) = 0.45$).

Experimental

Experiments were conducted with an FT-IR (Varian Excalibur series 3100) equipped with a high sensitivity mercury-cadmium-telluride (MCT) detector cooled with liquid nitrogen. In a first series of tests, the FT-IR was used with a gas flow cell located in its sample compartment as shown in Figure 1. The IR beam coming from the interferometer was transmitted through the gas flow cell and the absorbance spectrum was measured by the MCT detector. Before each experiment, a background spectrum was measured by flushing the gas flow cell with air and by coadding 20 spectra. Then, a gas/solid system was simulated in the FT-IR sample compartment by injecting a mixture containing 1.8 vol % C_3H_8 in air inside the gas flow cell and by placing a metal mesh (open area ratio of 16% and thickness of 1 mm) in the path of the IR beam.

A second series of experiments were performed with a mid-IR fiber-optic probe. In situ measurements of gaseous

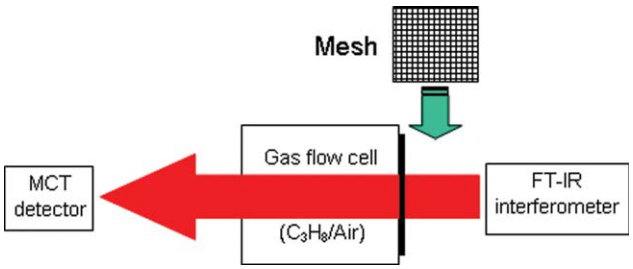

Figure 1. FT-IR instrument schematic.

[Color figure can be viewed in the online issue, which is available at wileyonlinelibrary.com.]

species composition and solids volume fraction were conducted inside a gas/solid flow of CH_4/N_2 mixtures and silica sand particles ($d_p = 290$ μm). A schematic of the apparatus is shown in Figure 2. The probe was composed of two parallel fluoride glass fiber-optics (an emitting and a receiving fiber-optic) with a numerical aperture of 0.2 and a core diameter of 600 μm. The fiber-optic probe was connected to the FT-IR with a Harrick Fibremate^{TM}. A planar gold-coated mirror was positioned perpendicularly to the probe tip at a distance of 5 mm. The mirror reflected the emitted IR beam to the receiving fiber-optic, which resulted in a measurement volume between the probe tip and the mirror as shown in grey on Figure 2. Experiments were conducted by first measuring a background spectrum—a CH_4/N_2 mixture was injected inside the measurement and a background spectrum was obtained from the coaddition of 20 spectra. Then, the measurement volume was flushed with air and the funnel was filled with sand particles to initiate a flow of solids. Absorbance spectra were measured at a frequency of 4.5 Hz (temporal resolution of 0.22 s) and the methane molar fraction was measured simultaneously to the solids volume fraction. The flow of solid particles was varied by changing the diameter of the funnel diameter at its throat. The corresponding solids volume fraction for each throat diameter was measured with a conventional back-scattering fiber-optic probe between the IR probe and the mirror. Four solids volume fractions were used: 0, 0.015, 0.038, and 0.097. Furthermore, four different CH_4/N_2 compositions were injected from calibrated gas cylinder in the measurement volume: 0, 0.1, 3.25, and 10.1 vol %.

Gas tracer experiments were also conducted in a small scale fluidized bed reactor (ID = 5 cm) illustrated in Figure 3 and the fiber-optic probe was used to measure the tracer molar fraction inside the bubble and emulsion phases. The reactor was filled with FCC particles ($d_p = 83$ μm and 14% fines ($d_p \leq 44$ μm)) and was fluidized with nitrogen at a superficial gas velocity of 2.6 mm/s ($U_{mf} = 2.5$ mm/s and $U_{mb} = 2.7$ mm/s). The expanded bed height was 12.5 cm and the fiber-optic probe was inserted in the bed at a height of 7 cm. A mirror was positioned perpendicularly at the probe tip and gas bubbles were produced in the fiber-optic probe measurement volume by injecting a mixture containing 10.1% CH_4 + 89.9% N_2 through a downward facing sparger. The CH_4/N_2 mixture was injected at a flow rate of 10 mL/s by manually opening a toggle valve for roughly 0.5 s at an interval of ~11 s.

Results and Discussion

During transmission spectroscopy in a gas/solid sample, both solid particles and gaseous species contribute to the absorbance spectrum, according to Eq. 1: the total absorbance at wavelength λ has a contribution from the solids volume fraction and from the gaseous species composition. Solid particles reduce the incident beam intensity by absorption, reflection, and diffusion. Solids can also influence the path length and sample volume such that the absorbance because of the chemical species is a function of solids volume fraction.

$$A_{\text{Total},\lambda} = A_{(1-\varepsilon),\lambda} + A_{Y_i,\lambda}[\text{fn}(1-\varepsilon)] \quad (1)$$

In the specific case of transmission spectroscopy where the effect of solids fraction on path length and sample volume can be neglected, Eq. 1 can be simplified to:

$$A_{\text{Total},\lambda} = A_{(1-\varepsilon),\lambda} + A_{Y_i,\lambda} \quad (2)$$

Equation 2 is valid when the reflected or diffused beam intensity measured is negligible compared with the transmitted light intensity. In Eq. 2, the effects of solids volume

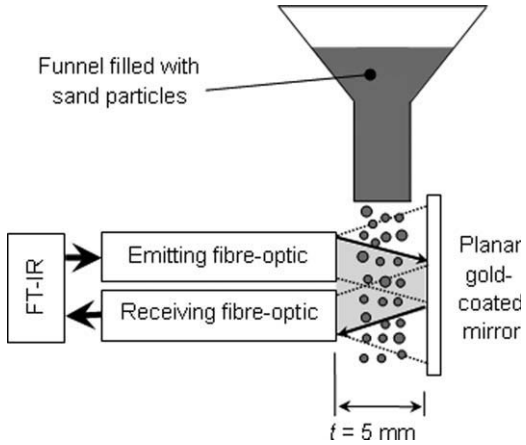

Figure 2. Fiber-optic probe apparatus schematic.

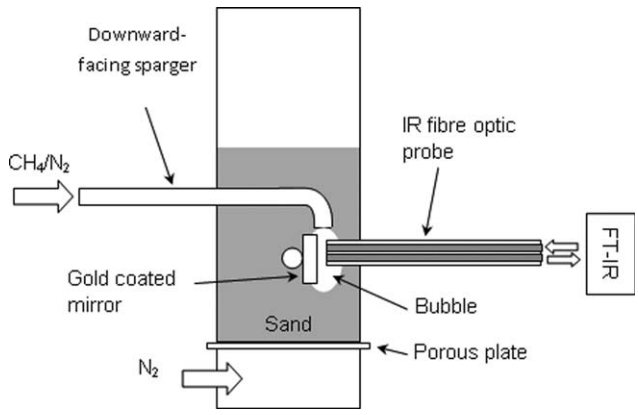

Figure 3. Fluidized bed reactor.

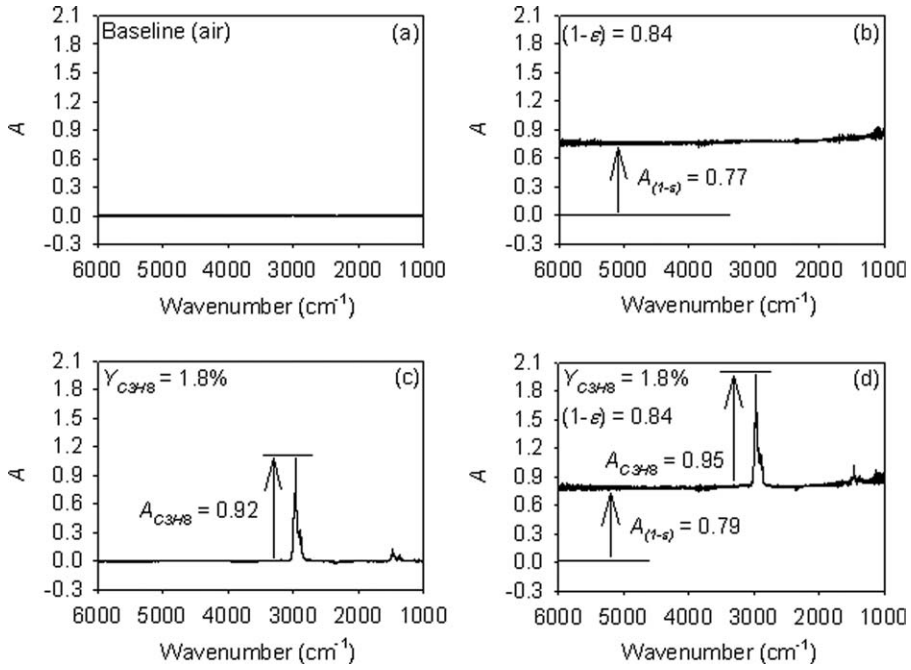

Figure 4. Simultaneous measurement of Y_{C_3H8} and $(1 - \varepsilon)$.

fraction and gaseous species composition on the absorbance spectrum are independent. Therefore, the effect of $(1-\varepsilon)$ and Y_i can be calibrated independently.

Experiments with the FT-IR

A first series of experiments were conducted with the FT-IR of Figure 1. A background spectrum of air was taken and four absorbance spectra were subsequently measured for the following conditions:

- Air and $(1-\varepsilon) = 0$ (Figure 4a)
- Air and $(1-\varepsilon) = 0.84$ (Figure 4b)
- 1.8% C_3H_8 + 98.2% air and $(1-\varepsilon) = 0$ (Figure 4c)
- 1.8% C_3H_8 + 98.2% air and $(1-\varepsilon) = 0.84$ (Figure 4d)

Figure 4a shows the absorbance spectrum of air, which corresponded to the background absorbance spectrum and resulted in a baseline of zero absorbance. Two calibration absorbance spectra were measured to independently evaluate the effect of the propane molar fraction and the solids volume fraction. The absorbance spectrum for air and a solids volume fraction of 0.84 is shown in Figure 4b—the baseline absorbance increased almost uniformly across the spectrum from to zero to a higher absorbance. The average baseline absorbance was 0.77 in the region of 3436.90–3427.98 cm^{-1}. This specific range of wavenumbers (3436.90–3427.98 cm^{-1}) was chosen to evaluate the average baseline absorbance as it was characterized by a good signal-to-noise ratio and as it was not absorbed by propane. The second calibration spectrum was obtained by injecting a mixture of 1.8% C_3H_8 in air inside the gas flow cell and by removing the metal mesh from the sample compartment. The injection of C_3H_8 resulted in the formation of two absorbance peaks at 2967.96 and 1471.68 cm^{-1}, as illustrated in Figure 4c. The average peak height of the tallest peak (at 2967.96 cm^{-1}) was measured as 0.92 in the region of 2969.65–2966.27 cm^{-1}.

Finally, the propane concentration and the solids volume fraction were measured simultaneously. The mixture of 1.8% C_3H_8 was injected inside the gas flow cell and the metal mesh was inserted inside the sample compartment. The resulting absorbance spectrum corresponded to the addition of both calibration spectra as observed in Figure 4d: the baseline absorbance was 0.79 (compared with 0.77) and the average C_3H_8 peak height above the baseline was 0.95 (compared with 0.92). Therefore, the propane concentration and solids volume fraction were measured simultaneously with a relative error of ~3% if a linear relation between absorbance and the two parameters is assumed. Equation 2 was valid in that particular case as the metal mesh had no appreciable influence on the path length of the IR beam—the path length was defined by the width of the sample compartment.

Experiments with the fiber-optic probe

A fiber-optic probe was built to conduct in situ measurements of solids volume fraction and species concentrations inside a flow of silica sand particles. Using the fiber-optic probe resulted in a significant loss in IR beam intensity, which occurred most likely at the probe tip. However, some signal loss probably occurred at the FT-IR/probe interface (Harrick Fibremate™) as well. Designing a system to yield a sufficiently intense transmitted IR beam was a challenge. The first fiber-optic probe prototype was built with two fiber-optics with a core diameter of 300 μm and no IR signal was ever measured by the FT-IR. The feasibility of using a more powerful external IR source was examined, but the coupling of the IR beam with the FT-IR interferometer proved to be particularly complex and yielded a significant risk of reducing the IR beam intensity below that of the internal FT-IR source. The installation of an external source was therefore abandoned. The construction of a new probe

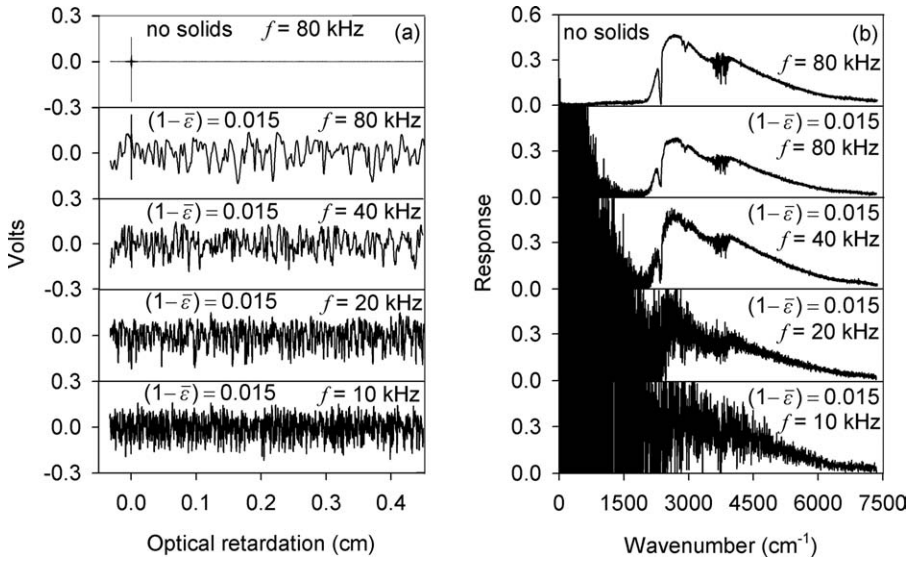

Figure 5. Effect of particle movement: (a) typical interferograms for moving particles; (b) corresponding single-beam spectra.

with core diameters of 600 μm and a complete realignment of the FT-IR increased the transmitted IR beam intensity sufficiently to perform the current experiments.

Another means of increasing the IR signal intensity consisted of installing a more sensitive detector. Indium antimonide (InSb) detectors can offer higher signal-to-noise ratios compared with MCT detectors at the wavenumbers of interest in the present study and an InSb detector was therefore tested. However, the selected InSb detector functioned at relatively low modulation frequencies (5–10 kHz) compared with the MCT detector (5–80 kHz) and this proved to be problematic in gas/solid systems where particles are moving. Particle movement produced artifacts (noise) in the interferograms and absorbance spectra and an initial analysis was performed to eliminate the artifacts from the wavenumbers of interest.

Effect of Particle Movement. Figure 5(a) shows typical interferograms measured with the fiber-optic probe in air at different modulation frequencies and two solids volume fractions. In the absence of solid particles, the interferogram was characterized by a centerburst at an optical retardation of 0 cm and a signal decay at higher retardation. With a flow of solids in the probe measurement volume that corresponded to a time-average solids volume fraction $(1-\bar{\varepsilon})$ of 0.015, fluctuations in the signal appeared. The number of fluctuations decreased as the modulation frequency (f) was increased from 10 to 80 kHz. Figure 5(b) shows the corresponding single-beam spectra. In the absence of solid particles, the spectrum was characterized by a reasonably high signal-to-noise ratio (S/N) over the entire spectrum. However, with a flow of solids and $(1-\bar{\varepsilon}) = 0.015$, noise was observed in the regions of low wavenumber (high wavelength and low frequency). The noise was produced by temporal variations in transmitted IR beam intensity because of heterogeneities in the gas/solid flow. As the modulation frequency was increased from 10 to 80 kHz, the noise moved to lower wavenumbers (higher wavelengths and lower frequencies). The modulation frequency corresponds to the number of displacements of 632.8 nm (equal to the laser wavelength) the moving mirror makes in 1 s in the interferometer. As the mirror speed was increased, a growing number of wavenumbers were modulated to frequencies that were significantly higher than the frequency at which the moving silica particles changed the transmitted IR beam intensity. At high wavenumbers (high frequency), the signal amplitude remained largely unaffected by the movement of particles. At a modulation frequency of 80 kHz, the artifacts were outside the wavenumber range of interest (2700–3300 cm^{-1}) and all experiments were therefore performed with this setting. Tests were also performed at higher solids volume fractions with no significant effect on the location of the fluctuations observed in the spectra.

Simultaneous Measurement of Methane Concentration and Solids Volume Fraction The fiber-optic probe was used to measure in situ absorbance spectra across the flow of sand particles. IR spectroscopy is based on the ratio of the background and the measured spectra. Experimentally, it was simpler to measure a background spectrum with a mixture of CH_4/N_2 (without solid particles) and conduct the experiments with a flow of particles in air such that negative CH_4 absorbance peaks were obtained. However, the methane molar fractions are reported as positive values in the present document. The results were unaffected by this procedure as the IR path length and measurement volume were independent of the solids volume fraction. When the mirror was removed from the tip of the probe, the signal amplitude measured by the MCT detector was zero. Therefore, the IR beam collected by the receiving fiber-optic did not have any contribution from diffuse reflectance on the solids surface and the probe measurement volume was only defined by the mirror position. Furthermore, the effects of methane concentration and solids volume fraction on the absorbance spectrum were independent.

A calibration was first performed with the fiber-optic probe to evaluate the effect of methane molar fraction and solids volume fraction on the absorbance spectrum. The

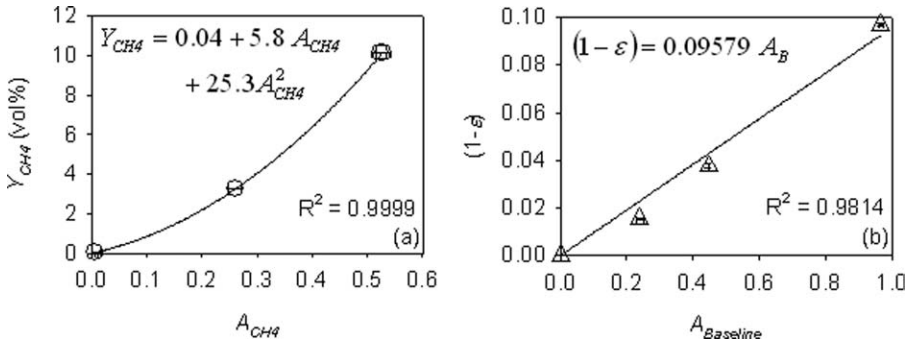

Figure 6. Fiber-optic probe calibration.

effect of methane molar fraction (Y_{CH_4}) was calibrated with four mixtures containing 0, 0.1, 3.25, and 10.1 vol % of methane in nitrogen. The apex of the methane peak (A_{CH_4}) was located at a wavenumber of 3017.63 cm^{-1} and its average absorbance was measured in the region of 3018.96–3016.86 cm^{-1}. The average absorbance in the region of 3018.96–3016.86 cm^{-1} is shown as a function of methane molar fraction in Figure 6a. The relationship between absorbance and Y_{CH_4} was nonlinear, but such a deviation from the Beer Law is common in IR spectroscopy.[40]

The effect of solids volume fraction was calibrated by varying the solids flow in the fiber-optic measurement volume. Four solids volume fractions were used (0, 0.015, 0.038, and 0.097) and the average baseline absorbance ($A_{(1-\varepsilon)}$) was measured in the regions of 2997.73–2992.04, 3036.70–3030.72, and 3045.87–3040.39 cm^{-1} during 75 s at a frequency of 4.5 Hz. This range of wavenumbers was chosen to evaluate the average baseline absorbance as it was characterized by a good signal-to-noise ratio and as it was not absorbed by methane. Figure 7 shows the history of the baseline absorbance for three solid flows that corresponded to time-averaged solids volume fractions of 0, 0.015, and 0.097. The measured absorbance fluctuated because of heterogeneities in the flow of solids. The average baseline absorbance is shown in Figure 6b as a function of solids volume fraction and the relationship is close to linear. Cutolo et al.[8] previously reported a linear relationship between absorbance and solids volume fractions. In the present case, solids volume fraction was measured by a conventional back-scattering fiber-optic probe with a different measurement volume compared with the IR fiber-optic probe. As the solids volume fraction was not completely constant across the flow of sand particles produced by the funnel, this may explain the observed deviation from the linear relationship.

Finally, the methane concentration and the solids volume fraction were simultaneously measured in the system. A background spectrum was first taken with a mixture containing 3.25% CH_4 in nitrogen. Then, a flow of sand particles that corresponded to a time-averaged solids volume fraction of 0.015 was initiated in air. Absorbance spectra were measured in real-time for 75 s and at a frequency of 4.5 Hz (temporal resolution of 0.22 s). Figure 8(a) shows the average baseline absorbance ($A_{(1-\varepsilon)}$) and average methane peak absorbance (A_{CH_4}) as a function of time for run #2 (Table 1). Both $A_{(1-\varepsilon)}$ and A_{CH_4} fluctuated with time around time-averaged values of 0.26 and 0.19, respectively. The calibrations (Figure 6) were used to calculate the instantaneous methane molar fraction (Y_{CH_4}) and solids volume fraction ($1-\varepsilon$) at each time interval. Figure 8(b) shows the calculated Y_{CH_4}

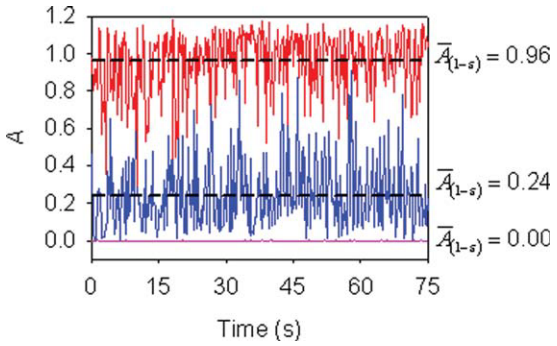

Figure 7. Solids volume fraction measurement.

[Color figure can be viewed in the online issue, which is available at wileyonlinelibrary.com.]

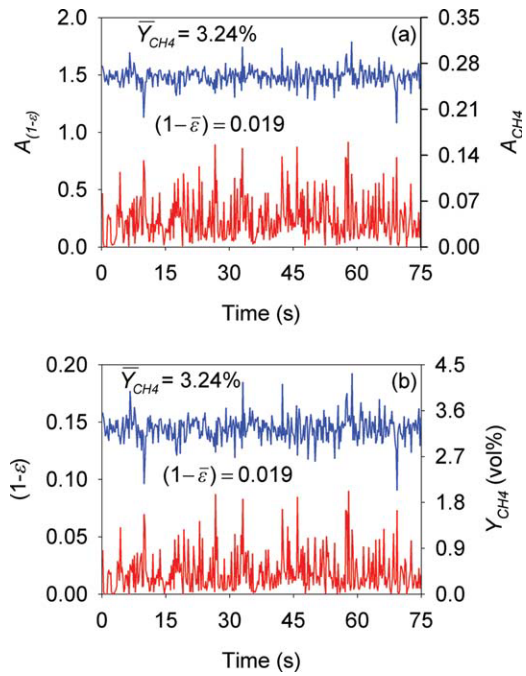

Figure 8. Simultaneous measurement of $(1-\varepsilon)$ and Y_{CH_4}.

[Color figure can be viewed in the online issue, which is available at wileyonlinelibrary.com.]

Table 1. Simultaneous Measurement of Y_{CH_4} and $(1-\varepsilon)$

	Fed to system		Measurements			
					Percentage (%) of Y_{CH_4} measurements within a relative error of	
Run	Y_{CH_4} (%)	$(1-\varepsilon)$	Y_{CH4} (%)	$(1-\varepsilon)$	±5%	±10%
1	3.25	0.015	3.31	0.019	54	83
2	3.25	0.015	3.24	0.019	55	87
3	10.1	0.015	10.09	0.02	83	98
4	10.1	0.015	10.20	0.018	82	98
5	3.25	0.038	3.31	0.039	38	70
6	3.25	0.038	3.41	0.037	37	63
7	10.1	0.038	10.05	0.041	61	86
8	10.1	0.038	9.95	0.04	63	87
9	3.25	0.097	3.44	0.097	18	31
10	10.1	0.097	10.06	0.098	30	55

and $(1-\varepsilon)$ as a function of time: both measurements fluctuated, but the time-averaged values were very close to the real values: 3.24% (compared with the real value of 3.25%) and 0.019 (compared with the real value of 0.015).

Figure 9 shows the measured methane molar fraction as a function of time and four horizontal lines represent the 5 and 10% relative deviation from the real value (3.25% CH_4). A majority of data points (55%) were within 5% of the real value. Furthermore, 87% of data points had a relative error of 10% or less.

Table 1 lists the experiments where solids volume fraction and methane concentration were measured simultaneously. The methane molar fractions and solids volume fractions fed to the system are listed for each run as well as the measured time-averaged values obtained from the absorbance spectra. The measured time-averaged solids volume fraction $(1-\bar{\varepsilon})$ and methane molar fraction $(\overline{Y}_{CH_4})$ were all very close to the real values: the maximum relative error on the measured $\overline{Y}_{CH_4}$ was 5.8% (run #9). Table 1 also shows the percentage of data points that had a relative error in the measured $\overline{Y}_{CH_4}$ of 5 and 10% or less—this percentage decreased with increasing solids volume fraction. Increasing the solids volume fraction decreased the accuracy of the real-time and time-averaged Y_{CH_4} measurements.

Effects of the Transmitted IR Beam Intensity on the Y_i Measurement Error. As the solids volume fraction increased, the intensity of the transmitted IR beam decreased and the signal-to-noise ratio (*S*/*N*) of the FT-IR decreased accordingly. Figure 10a was obtained by taking a background spectrum of a mixture of 3.25% CH_4 in nitrogen and measuring the absorbance spectra of air with two time-averaged solids volume fractions (0 and 0.015). Figure 10a shows that a time-averaged solids volume fraction of 0.015 resulted in a significantly lower *S*/*N* and the fluctuations of the baseline were of the same order as the methane peak (located at 3017.63 cm^{-1}).

The intensity of the IR beam is a concern with fiber-optic probes as their use significantly reduces the effective IR signal. Figure 10b shows the single beam spectrum of the FT-IR and the fiber-optic probe for air and $(1-\varepsilon) = 0$: the IR signal intensity was reduced by a factor of ~288 when the fiber-optic probe was installed. Note that the sensitivity of the MCT detector had to be increased by a factor of 16 with the fiber-optic probe.

For each experimental run listed in Table 1, the variance (σ) of the methane molar fraction measurements was calculated. Figure 11 shows the variance as a function of time-average solids volume fraction and methane molar fraction: increasing the solids volume fraction greatly increased the variance. This strongly suggests that the accuracy of the fiber-optic probe measurements can be improved by increasing the IR beam intensity. This could be achieved by using a fiber-optic bundle, optimizing the signal transmission at the probe tip and at the FT-IR/fiber-optic probe interface (Harrick Fibremate™). The effect of decreasing *S*/*N* could also be minimized by improving the curve smoothing technique to evaluate the baseline absorbance.

Real-Time and Time-Averaged Y_i Measurements. Real-time Y_{CH_4} measurements were characterized by greater errors than the time-averaged values. For example, Figure 9 shows instantaneous Y_{CH_4} measurements with relative errors of more than 10% while the error on the time-averaged Y_{CH_4} measurement (Table 1—run #2) was less than 1%. Furthermore, the maximum relative error on the time-averaged Y_{CH_4} measurements was 5.8% (run #9). Applied to a multiphase reactor, the present method could measure precisely the time-averaged chemical species composition inside the regions of relatively low solids volume fractions. The technique can also be more sensitive to lower $(1-\varepsilon)$ and Y_i measurements by increasing the IR beam path length (*t*). As an average species composition between the dense and dilute phases can be measured by using a sampling probe and analyzing the samples, the

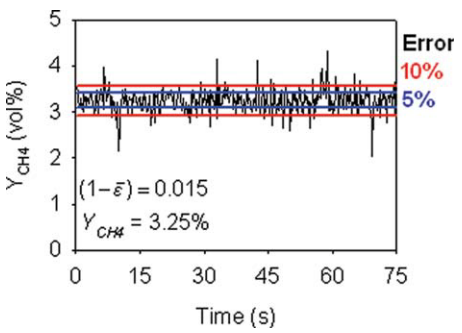

Figure 9. Error on Y_{CH_4} measurement.

[Color figure can be viewed in the online issue, which is available at wileyonlinelibrary.com.]

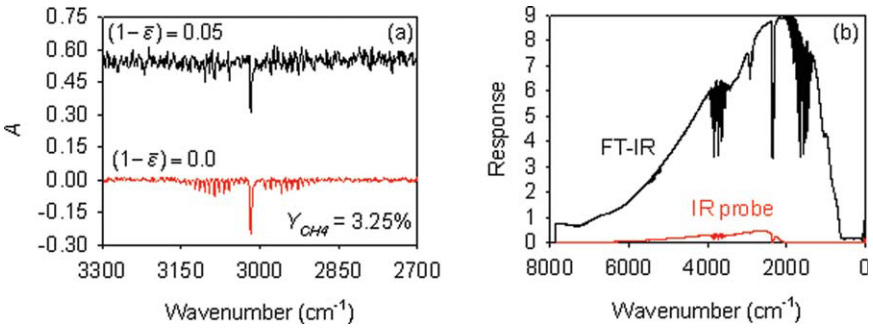

Figure 10. Source of error on Y_{CH_4} measurements.

[Color figure can be viewed in the online issue, which is available at wileyonlinelibrary.com.]

chemical composition in the dense phase could be calculated by subtracting the dilute phase composition from the average (dilute and dense phases) composition.

Application in fluidized beds—chemical composition measurement in the bubble phase

Gas tracer experiments were conducted in a fluidized bed and the fiber-optic probe was used with the spectroscopic method to measure the molar fraction of a CH_4 tracer inside the bubble and emulsion phases. A bed of FCC particles was incipiently fluidized with nitrogen and bubbles were produced at the tip of the fiber-optic probe by the injection of a nitrogen/methane mixture (10.1% CH_4) through a sparger. Figure 12 shows the history of solids volume fraction and methane molar fraction measured by the fiber-optic probe during a typical experiment: the solids volume fraction was 0.45 in the emulsion phase and decreased significantly to 0.05–0, when gas bubbles of CH_4/N_2 were injected at intervals of ~11 s. The measured methane volume fraction in the emulsion phase fluctuated significantly (5 to −5%) because of the low intensity of the transmitted IR beam and the resulting low *S*/*N*. Figure 13(a) shows a typical absorbance spectrum measured in the emulsion phase: the low intensity of reflected signal resulted in a high absorbance throughout the spectrum. However, the time-average methane molar fraction was measured accurately as 0.0% (100% nitrogen).

Figure 13(b) shows an absorbance spectrum measured inside a bubble: a methane peak was observed at 3017.63 cm^{-1}. However, the injection of bubbles produced gas/solids movement, which caused noise in most recorded absorbance spectra: five spectra of the 27 measured in the bubble phase were sufficiently clear to make a measurement of Y_{CH_4}. Figure 13(c) shows a typical absorbance spectrum where noise was observed and the methane peak was indistinguishable. This noise could be eliminated in the wavelengths of interest by using a FT-IR with a higher modulation frequency.

The average peak height measured in the bubble phase corresponded to a methane molar fraction of 5% compared with the injected 10.1% CH_4 in nitrogen. This discrepancy may be due to mixing at the injector tip between the gas injected through the sparger and the fluidizing gas. Furthermore, the small number of clear spectra that were measured in the bubble phase could also explain the low value of Y_{CH_4} measured as time-average measurements were more accurate than instantaneous measurements. During the present study, the measured absorbance spectra had to be exported and analyzed manually, which greatly reduced the number of spectra that could be considered to measure Y_{CH_4} in the bubble phase. However, these results clearly show that the developed spectroscopic method with a fiber-optic probe can measure the gas composition in the bubble phase.

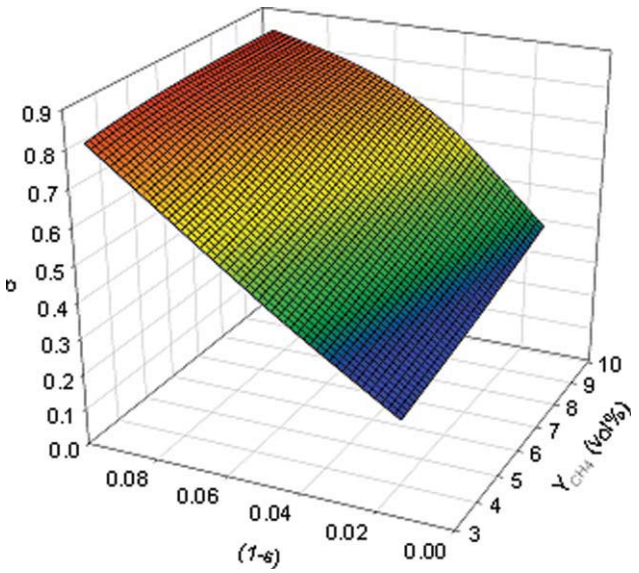

Figure 11. Effect of $(1-\varepsilon)$ and Y_{CH_4} on the variance of Y_{CH_4}.

[Color figure can be viewed in the online issue, which is available at wileyonlinelibrary.com.]

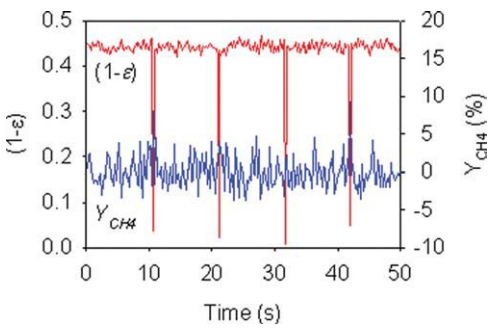

Figure 12. Simultaneous measurement of Y_{CH_4} and $(1-\varepsilon)$ in the fluidized bed.

[Color figure can be viewed in the online issue, which is available at wileyonlinelibrary.com.]

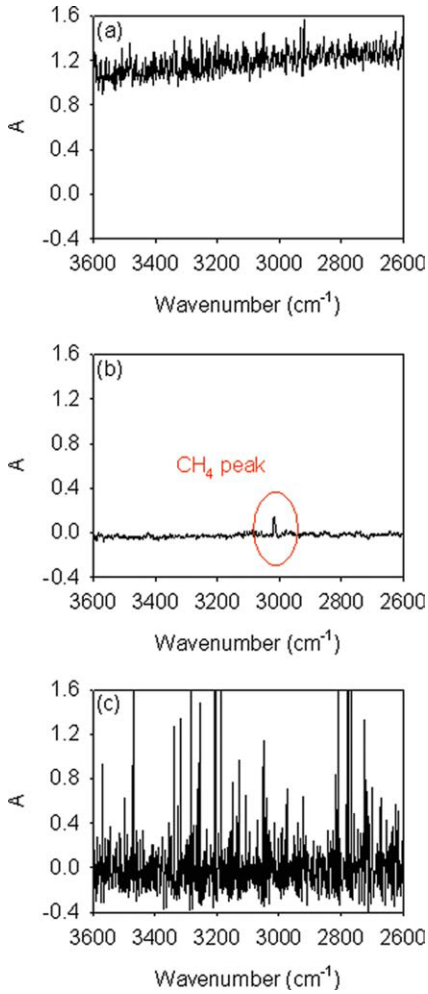

Figure 13. Absorbance spectra in the emulsion and bubbles phases.

[Color figure can be viewed in the online issue, which is available at wileyonlinelibrary.com.]

Limitation of the technique and future work

This measurement technique is limited by the modulation frequency of the spectrometer: the modulation frequency needs to be sufficiently high to avoid noise in the absorbance spectrum because of the movement in the gas/solid system. The FT-IR used in the present study was purchased in 2001 and new models are currently available with significantly higher modulation frequencies.

Another limitation of the technique is the IR beam intensity transmitted in the fiber-optic probe, which needs to be as high as possible to maximize the signal-to-noise ratio. This is critical if instantaneous measurements are required. On the other hand, time-averaged measurements have been shown in the present study to be much more accurate with lower IR beam intensity. The IR beam intensity can be increased by using a fiber-optic bundle, using a more sensitive detector, using a more powerful IR source and optimizing the signal transmission at the probe tip and at the FT-IR/fiber-optic probe interface (Harrick Fibremate^{TM}). More recent models of FT-IR also propose higher IR signal intensity compared to the equipment used in the present study.

The fiber-optic probe used in this study is limited to ambient temperature applications: fluoride glass fiber-optics used can be exposed to temperatures below 150°C. However, fiber-optic probes have been developed with plastic fiber-optics for temperatures up to 1000°C.[41] Therefore, it is reasonable to assume that the measurement technique could be used to perform in situ measurements in high temperature multiphase systems with an adequately designed fiber-optic probe.

Conclusions

A novel spectroscopic method was developed to measure quantitatively and simultaneously solids volume fraction $(1-\varepsilon)$ and gaseous species composition (Y_i) in a gas/solid system. The method was comprised of an FT-IR coupled to a fiber-optic probe that could perform real-time and in situ measurements of absorbance. The effect of solids volume fraction and gaseous chemical composition on the absorbance spectra were additive and could be independently calibrated. Experiments were conducted with methane/nitrogen and propane/nitrogen mixtures and two types of particles: sand and FCC. Fuel mole fraction and solids volume fraction were varied between 1.8–10.1 mol % and 0–0.45, respectively. The relative errors for the time-averaged measurements of gaseous species mole fraction were below 6% and the error increased significantly with decreasing beam intensity. The fiber-optic probe was also used in a fluidized bed to measure the molar fraction of a gas tracer inside the emulsion and bubble phases during gas tracer experiments.

The results strongly suggest that the accuracy of instantaneous fiber-optic probe measurements could be significantly improved by increasing the IR beam intensity. This could be achieved by using a fiber-optic bundle, using a more sensitive detector, using a more powerful IR source and optimizing the signal transmission at the probe tip and at the FT-IR/fiber-optic probe interface (Harrick Fibremate^{TM}). New FT-IR models also propose significantly higher IR signal intensity compared with the equipment used in the present study. The effect of decreasing signal-to-noise ratio could also be minimized by improving the curve smoothing technique to evaluate the baseline absorbance.

More measurements need to be performed in gas/solid systems at ambient and high temperatures to fully demonstrate the possibilities of this measurement method. High modulation frequencies from newer models of FT-IR should help resolve the problem of noise in the absorbance spectra caused by gas/solid movement. In theory, this method could also be used for liquid/solid, gas/liquid, liquid/liquid, and gas/liquid/solid systems. However, work has to be performed to identify the limitations in these specific systems.

Acknowledgments

The authors are grateful to the Natural Sciences and Engineering Research Council of Canada (NSERC) for their financial support. The authors would also like to thank IRphotonics for their assistance in the fiber-optic probe construction.

Notation

A = absorbance
d_p = average particle size (μm)
f = modulation frequency (kHz)

t = distance between probe tip and mirror (mm)
Y_i = molar fraction of specie i (vol %)

Greek letters

$(1-\varepsilon)$ = solids volume fraction
λ = wavelength (μm)
σ = Variance

Literature Cited

1. Werther J, Molerus O. The local structure of gas fluidized beds—I. A statistically based measuring system. *Int J Multiphase Flow*. 1973;1:103–122.
2. Yates JG, Simons SRJ. Experimental methods in fluidization research. *Int J Multiphase Flow*. 1994;20:297–330.
3. Hage B, Werther J. The guarded capacitance probe—a tool for the measurement of solids flow patterns in a laboratory and industrial fluidized bed. *Powder Technol*. 1997;93:235–245.
4. Begovich J, Watson JS. An electroconductivity technique for the measurement of axial variation of hold-ups in three-phase fluidized beds. *AIChE J*. 1978;24:351–354.
5. Uribe-Salas A, Gomez CO, Finch JA. A conductivity technique for gas and solids holdup determination in three-phase reactors. *Chem Eng Sci*. 1994;49:1–10.
6. Liu M, Wang T, Yu W, Wang J. An electrical conductivity probe method for measuring the local solid holdup in a slurry system. *Chem Eng J*. 2007;132:37–46.
7. Huizenga P, Meijer R, Kuipers JAM, van Swaaij WPM. Fluoroptic solids holdup measurements in slurry systems. *AIChE J*. 1998;44:982–988.
8. Cutolo A, Rendina I, Arena U, Marzocchella A, Massimilla L. Opto-electronic technique for the characterization of high concentration gas-solid suspension. *Appl Opt*. 1990;29:1317–1322.
9. Ishida M, Tanaka H. Optical probe to detect both bubbles and suspended particles in a three-phase fluidized bed. *J Chem Eng Japan*. 1982;15:389–391.
10. Hu T, Yu B, Wang Y. *Holdups and models of three phase fluidized beds*. In: Ostergaard K, Sorensen A, editors. *Fluidization V*. New York: Engineering Foundation, 1986: 353.
11. Esmaeili B, Chaouki J, Dubois C. An evaluation of the solid holdup distribution in a fluidized bed of nanoparticles using radioactive densitometry and fibre optics. *Can J Chem Eng*. 2008;86:543–552.
12. Gandhi B, Prakash A, Bergougnou MA. Hydrodynamic behaviour of slurry column at high solids concentrations. *Powder Technol*. 1999; 103:80–94.
13. Chaouki J, Larachi F, Duduković MP. Noninvasive tomographic and velocimetric monitoring of multiphase flows. *Ind Eng Chem Res*. 1997;36:4476–4503.
14. Pugsley T, Tanfara H, Malcus S, Cui H, Chaouki J, Winters C. Verification of fluidized bed electrical capacitance tomography measurements with a fibre optic probe. *Chem Eng Sci*. 2003;58:3923–3934.
15. Marashdeh Q, Fan LS, Du B, Warsito W. Electrical capacitance tomography—a perspective. *Ind Eng Chem Res*. 2008;47:3708–3719.
16. Razzak SA, Barghi S, Zhu JX, Mi Y. Phase holdup measurements in a gas-liquid-solid circulating fluidized bed (GLSCFB) riser using electrical resistance tomography and optical fibre probe. *Chem Eng J*. 2009;147:210–218.
17. Uchida S, Okamura S, Katsumata T. Measurement of longitudinal distribution of solids holdup in a three-phase fluidized bed by ultrasonic technique. *Can J Chem Eng*. 1989;67:166–169.
18. Luypaert J, Massart DL, Vander Heyden Y. Near-infrared spectroscopy applications in pharmaceutical analysis. *Talanta*. 2007;72: 865–883.
19. Swarbrick B. Process analytical technology: a strategy for keeping manufacturing viable in Australia. *Vib Spectrosc*. 2007;44:171–178.
20. Armaroli T, Bécue T, Gautier S. Diffuse reflection infrared spectroscopy (drifts) : application to the in situ analysis of catalysts. *Oil Gas Sci Technol*. 2004;59:215–237.
21. Kondo JN, Yang S, Zhu Q, Inagaki S, Domen K. In situ infrared study of n-heptane isomerization over Pt/H-beta zeolites. *J Catal*. 2007;248:53–59.
22. Corveleyn S, Vandenbossche GMR, Remon JP. Near-infrared (NIR) monitoring of H_2O_2 vapor concentration during vapour hydrogen peroxide (VHP) sterilisation. *Pharm Res*. 1997;14:294–298.
23. Rantanen J, Räsänen E, Tenhunen J, Känsäkoski M, Mannermaa J-P, Yliruusi J. In-line moisture measurement during granulation with a four-wavelength near infrared sensor: an evaluation of particle size and binder effects. *Eur J Pharm Biopharm*. 2000a;50:271–276.
24. Rantanen J, Antikainen O, Mannermaa J-P, Yliruusi J. Use of the near-infrared reflectance method for measurement of moisture content during granulation. *Pharm Dev Technol*. 2000;5:209–217.
25. Cogdill RP, Anderson CA, Delgado M, Chisholm R, Bolton R, Herkert T, Afnan AM, Drennen JK III. Process analytical technology case study part I: feasibility studies for quantitative near-infrared method development. *AAPS PharmSciTech*. 2005;6:E273–E283.
26. Triadaphillou S, Martin E, Montague G, Norden A, Jeffkins P, Stimpson S. Fermentation process tracking through enhanced spectral calibration modeling. *Biotechnol Bioeng*. 2007;97:554–567.
27. Andersson M, Josefson M, Langkilde FW, Wahlund K-G. Monitoring of a film coating process for tablets using near infrared reflectance spectrometry. *J Pharm Biomed Anal*. 1999;20:27–37.
28. Kirsch JD, Drennen JK. Determination of film-coated tablet parameters by near-infrared spectroscopy. *J Pharm Biomed Anal*. 1995; 13:1273–1281.
29. Kirsch JD, Drennen JK. Near-infrared spectroscopic monitoring of the film coating process. *Pharm Res*. 1996;13:234–237.
30. Abrahamsson C, Johansson J, Andersson-Engels S, Svanberg S, Folestad S. Time-resolved NIR spectroscopy for quantitative analysis of intact pharmaceutical tablets. *Anal Chem*. 2005;77:1055–1059.
31. Hailey PA, Doherty P, Tapsell P, Oliver T, Aldridge PK. Automated system for the on-line monitoring or powder blending processes using near-infrared spectroscopy. Part I. system development and control. *J Pharm Biomed Anal*. 1996;14:551–559.
32. Sonja Sekulic S, Wakeman J, Doherty P, Hailey PA. Automated system for the on-line monitoring of powder blending processes using near-infrared spectroscopy: Part II. Qualitative approaches to blend evaluation. *J Pharm Biomed Anal*. 1998;17:1285–1309.
33. Sonja Sekulic S, Ward HW, Brannegan DR, Stanley ED, Evans CL, Sciavolino ST, Hailey PA, Aldridge PK. On-line monitoring of powder blend homogeneity by near-infrared spectroscopy. *Anal Chem*. 1996;68:509–513.
34. Frake P, Greenhalgh D, Grierson SM, Hempenstall JM, Rudd DR. Process control and end-point determination of a fluid bed granulation by application of near infra-red spectroscopy. *Int J Pharm*. 1997;151:75–80.
35. Bellamy LJ, Nordon A, Littlejohn D. Real-time monitoring of powder mixing in a convective blender using non-invasive reflectance NIR spectrometry. *The Analyst*. 2008;133:58–64.
36. Cui H, Mostoufi N, Chaouki J. Comparison of measurement techniques of local particle concentration for gas-solid fluidization. In: Kwauk M, Li J, Yang W-C, editors. *Fluidization X*. New York: Engineering Foundation, 2001: 779–786.
37. De Paepe ATG, Dyke JM, Hendra PJ, Langkilde FW. Rotating samples in FT-RAMAN spectrometers. *Spec Acta Part A*. 1997;53: 2261–2266.
38. Berntsson O, Danielsson L-G, Folestad S. Characterization of diffuse reflectance fiber probe sampling on moving solids using a Fourier transform near-infrared spectrometer. *Anal Chim Acta*. 2001;431: 125–131.
39. Andersson M, Svensson O, Folestad S, Josefson M, Wahlund K-G. NIR spectroscopy on moving solids using a scanning grating spectrometer—impact on multivariate process analysis. *Chemometr Intell Lab Sys*. 2005;75:1–11.
40. Skoog DA, Holler FJ, Crouch SR. *Principles of Instrumental Analysis*, 6th Ed. Independence, KY: Brooks Cole, 2006.
41. Cui H, Sauriol P, Chaouki J. High temperature fluidized bed reactor: measurements, hydrodynamics and simulation. *Chem Eng Sci*. 2003; 58:1071–1077.

Manuscript received Apr. 28, 2009, revision received Nov. 29, 2009, and final revision received Feb. 10, 2010.